876

CDF/DOC/CDF/CDFR/2940

PROPOSAL FOR HARD DIFFRACTION STUDIES IN CDF[1]

The Hard Diffraction Group of CDF

M.Deninno
Instituto Nazionale di Fisica Nucleare, University of Bologna, Italy

M.G.Albrow, C.Moore
Fermi National Accelerator Laboratory

J.Huston
Michigan State University

G.Bellettini
Instituto Nazionale di Fisica Nucleare, University of Pisa, Italy

A.Akopian, G.Apollinari, S.Bagdasarov, A.Bhatti, L.Demortier,
N.Giokaris, K.Goulianos, D.Khazins, A.Maghakian, P.Melese, A. Titov, Q.Wang.
Rockefeller University

H. Ikeda, S.H.Kim, K.Kondo, Miyamoto
University of Tsukuba, Japan

H. Akimoto, T.Arisawa, Y. Fujimoto, S.Hasegawa, J.Iwai
Waseda University, Japan

January 17, 1995

[1]Subject to approval by the CDF collaboration

Contents

Abstract

As part of the studies of QCD in CDF, we propose to include hard and high mass diffraction. This program can be carried out in parallel with all current CDF physics investigations, as the rates are low and the standard low-β optics are used. We need to add a triplet of track detectors in Roman Pots in the downstream antiproton arm; this could be done during the shutdown scheduled for Summer 1995. In addition, we need to add small calorimeters to plug the holes between the beam pipe (0.5^0) and the forward calorimeters (2.5^0) in run IB, or the Upgraded Plug Calorimeters (3^0) in run II.

1 Introduction / Physics Motivation

Despite the great success of the Standard Model of the Electro-Weak theory and of Quantum Chromo-Dynamics (QCD), there are still many areas of particle physics where we have little or no understanding. Theorists are unable to make calculations in cases where the strong coupling becomes large and the perturbative calculations do not converge; they have to resort to making approximate calculations using very time-consuming techniques like lattice gauge theory or, alternatively, to phenomenology such as bag models for hadrons or Regge theory for reactions. These methods have their domains of applicability, but are very unsatisfactory for many reasons. Regge theory became too complicated when, to obtain good agreement with data, one had to add "cuts" (equivalent to multiple pole exchanges). Furthermore, it is difficult, at least for experimentalists, to visualize "trajectories in the plane of complex angular momentum" and such things; quarks and gluons seem much easier to picture. We behave as if we had in QCD a good theory of strong interactions; yet about 25% of the total $p\bar{p}$ cross section at the Tevatron is elastic scattering and we cannot calculate it. Another sizeable fraction, $\sim 10\%$, is diffractive excitation of one or both of the incoming hadrons; this is also not calculable in QCD. These processes are intimately related, with the "pomeron" exchanged between the hadrons. The pomeron carries 4-momentum from one hadron to the other, but we don't know what it really is, even if we know something of its phenomenology (such as its couplings and its propagator). It has the quantum numbers of the vacuum, and understanding it better might teach us something interesting about the vacuum, as well as about confinement and who knows what else.

We now have, in the Tevatron, a really good opportunity to do experiments to determine the nature of the pomeron. In good HEP tradition, we can make it collide with something we think we do understand and study the results. At the very high energy of the Tevatron, it is possible to use hard probes. Take single diffractive excitation as the prime test reaction: the antiproton emits a pomeron, $\mathcal{P}$, which interacts with the proton, exciting it into a high mass state. The masses M attainable reach of order 300 GeV, to be compared with 100 GeV at the CERN Collider and 10 GeV at the ISR, where it was discovered that one could excite the proton beyond the resonance region. Even higher masses are likely to be excited diffractively, but the background from non-diffractive processes then becomes relatively large. These limits correspond to $x_{\bar{p}} > 0.95$ where $x_{\bar{p}}$ is the fractional momentum of the scattered antiproton relative to its initial momentum, and $x_{\bar{p}} = 1 - M^2/s$. We can now picture this excitation as resulting from a $\mathcal{P}$p collision at $\sqrt{s}$=300 GeV and below, where $\mathcal{P}$ is (is it?) a quasi-particle with negative $mass^2$ (equal to t, the four-momentum transfer squared which, incidentally, we can vary; it is approximately $t = -p_T^2$). Hadron-hadron collisions at this $\sqrt{s}$, five times that of the ISR, show all the hard phenomena we can relate to the quark and gluon structure of the colliding hadrons, as for example high p_T jets. By measuring jet-pairs in pp or p$\bar{\text{p}}$ collisions one can extract an effective parton structure function for the proton $[Q(x) + 4/9G(x)]$. By measuring such jet pairs in $\mathcal{P}$p collisions, and knowing the p structure, we can extract an effective parton structure as a function of ξ, the momentum fraction of a parton in the pomeron, for the $\mathcal{P}$. This will not tell us whether it "contains" predominantly quarks or gluons - for that we need other measurements - but it should at least establish whether such a constituent picture has validity for $\mathcal{P}$ as it does for hadrons, and if so, is it a hard or a soft distribution, does it depend on mass and/or t, and so on. Such an experiment was done by UA8 at the CERN Collider [1] at a $\sqrt{s}$ three times lower than the Tevatron's. The experimenters observed rather clean (albeit rather low E_T) di-jet events and concluded that the structure function of $\mathcal{P}$ is hard, more like $\xi(1-\xi)$ rather than soft, like $(1-\xi)^5$. They also claim a significant (30%) delta-function-like component, which they call *superhard*, in which the entire momentum of $\mathcal{P}$ seems to participate in the hard scattering. However, in order to study "high" masses, they allowed the high-x proton to have x as low as 0.90 (M = 200 GeV), where the non-diffractive background (in the Regge picture, exchanges of meson trajectories) dominate over $\mathcal{P}$-exchange. In order to safely probe the pomeron, x should exceed $\sim$ 0.95, a region which is practically excluded from their study. If it is true that there is a delta-function-like component in the pomeron, it is a very important discovery; taken literally, it implies a colorless, pointlike (on the scale probed), strong or semi-strong exchange, which is not single gluon exchange. It clearly deserves further study by an independent experiment. The pomeron is then behaving like an isoscalar photon, an analogy which has been successfully exploited for soft diffraction [2]. This would have repercussions also in other processes, such as double diffraction dissociation (DDD), where both incoming hadrons get excited. The exchange of this "hard $\mathcal{P}$" could give events with two high p_T jets separated by a large rapidity gap, where there are no hadrons, as can happen with a colorless exchange. Such events have been observed by both CDF [3] [4] and D0 [5]. What is the relation between the very high t colorless exchange in our jet-gap-jet events and the claimed superhard pomeron of UA8?

Even though we do not now have detectors for the high-x proton, we have searched for diffractive production of di-jets by looking for rapidity gaps in events with two forward jets close in rapidity ("same-side jets") [4]. We see no evidence for such a gap signal and put a (95% CL) upper limit of 0.32% on the fraction of such di-jet events that are diffractive. This appears to be inconsistent with the UA8 results, although the discrepancy is not very significant. If it becomes significant with more data, there are at least two reasonable explanations. One is that the UA8 data are not in fact diffractive, the relatively low-x protons of that experiment ($0.90 \leq x \leq 0.95$) being mostly due to non-pomeron Regge exchanges (ρ, ω). This we can test because for the same diffractive mass at $\sqrt{s} = 1800$ GeV we have $x \sim 0.99$ rather than 0.90 and the pomeron dominates [6]. Another explanation is that pomeron interactions are t-dependent. Because in our CDF rapidity gap study we did not detect the quasi-elastic proton, we are integrating over its t, and the data are dominated by small t. It is conceivable that small-t pomerons couple predominantly to hadrons and larger t pomerons couple to quarks. The UA8 experiment could then be on the borderline, the pomeron with $1 \leq |t| \leq 2\ GeV^2$ coupling to the proton on one vertex and to a quark at the other. In the experiment we propose, at a fixed large mass $M = 300$ GeV we can scan from $t \approx 0$ (note that even with a 45 GeV energy loss for the antiproton the four-momentum transfer squared t can be much less than m_π^2) to $t = -5\ GeV^2$ and see if we observe a systematic change with t in the behavior of the pomeron.

We can unravel the nature of the pomeron "constituents" (assuming that it is a valid paradigm) and tell whether they are quarks or gluons by making other measurements. A classic study would be to measure Drell-Yan lepton pair production, say with pair masses between the J/ψ and the Υ (also below and above, if possible). This process measures the q-$\bar{\text{q}}$ product distribution. The observation of Drell-Yan pairs in high mass diffraction will be proof of the existence of q/$\bar{\text{q}}$ inside $\mathcal{P}$ (they must be there at some level even if only as a gluon-created sea). By measuring the mass and rapidity distributions of the lepton pairs we can obtain, by deconvoluting the proton structure function, the q/$\bar{\text{q}}$ distribution in the pomeron. It is also very interesting to see whether W's and Z's are produced diffractively with sufficient cross-section to be detectable. We have already carried out [7] a first search for diffractive W production using the rapidity gap method. We find a 95% CL upper limit on the fraction of W produced diffractively of 2.1%, to be compared with an estimate of 17-24% for a hard quark structure function of the pomeron of the form favored by UA8. As before, this applies to low-t pomerons.

At first it may seem very surprising that as many as about 20% of the produced W could possibly be diffractive, when the diffractive fraction of the inelastic cross section is somewhat less than this and the energy available for particle production is also much less in diffractive collisions than in the average inelastic collision. However pomerons could be very much more effective at producing hard parton interactions than protons are. The parton cross sections, $\sigma(gg \rightarrow Q\bar{Q})$ for example, are of course identical, but the pomeron may be very compact. Notice that the total cross section $\sigma(\mathcal{P}p)$ is only about 2 mb. By comparison, the proton is largely "empty space".

Another important measurement, which can be well done in CDF given the vertex detectors, is the production of heavy flavors, charm and beauty. In p-$\bar{\text{p}}$, these occur mostly through gg fusion reactions, and in $\mathcal{P}$p the rates will tell us about the gluon structure function of $\mathcal{P}$. In particular, if $\mathcal{P}$ is predominantly gluonic, high mass diffractive events could be relatively rich in heavy flavors. The simultaneous study of jets, lepton pairs and heavy flavors in high mass single diffraction excitation (SDE) will show whether a consistent picture emerges of $\mathcal{P}$ as an object with q/g constituents similar to a real hadron. We would measure different t and M^2 values at the same time, and could thus check scaling properties and so on. There is an extensive program of work, provided we can get enough data to do a thorough study. It may of course turn out that this attempt to understand $\mathcal{P}$ as if it were a real hadron with quark and gluon structure functions $Q(\xi, Q^2)$ and $G(\xi, Q^2)$ fails; i.e. that it is not self-consistent. Such an outcome would be just as interesting.

In order to carry out the measurements on single diffractive excitation physics, one needs to detect the quasi-elastically scattered (anti)proton. Quasi-elastic means $x >\sim 0.95$ and small p_T ($<\sim$ 2.5 GeV/c). This can be done by inserting precision track detectors in Roman Pots that can be moved close to the circulating beam, some 50 m downstream of B0 and after the scattered $\bar{\text{p}}$'s have traversed quadrupoles and dipoles. The track measurement there, together with the vertex of the interaction, gives the momentum. This information can be used to trigger on diffractive events, where the other proton is excited to a mass M, through the relation $M^2/s = (1 - x)$, where $x = p_{out}/p_{in}$ for the antiproton. Note that unlike the previous diffractive studies in CDF [6], we are only interested in high mass diffraction and do not need a *precision* measurement of the momentum transfer t. This should make life easier than in the earlier experiment: we can be farther away from the beams and halo should be less of a problem. The events in CDF should be full of activity mostly in the hemisphere opposite the antiproton, quite unlike "minimum bias" background. In particular a small angle calorimeter on the $\bar{p}$ side should contain very little energy. There should be a correspondence between the total mass detected in CDF (calculating "mass" from the calorimeter "energy vectors") and the missing mass to the antiproton (calculated from $x_{\bar{p}}$). It should be possible to get a clean sample of SDE events, although to determine exactly what fraction of the events correspond to $\mathcal{P}$-exchange (at a given M, t) rather than some other exchange (e.g. the ρ trajectory) might require some running at a different $\sqrt{s}$. We are not making a request for that now; there is an enormous amount to do at the standard Tevatron $\sqrt{s}$ of 1800/2000 GeV. However, we take note of the Proposal for a Special Run at $\sqrt{s}$ = 630 GeV (CDF/DOC/CDF/CDFR/2196) and we will be interested in it if we are installed at the time.

There is another diffractive reaction which might turn out to be extremely interesting, especially if $\mathcal{P}$ does indeed have a delta-function-like component, in which both beam hadrons emit $\mathcal{P}$'s which interact in the central region. This is the process known as Double Pomeron Exchange (DPE), which is like a diffractive excitation of the vacuum, Central Vacuum Excitation (CVE). The produced hadrons are mainly central and so CDF is well suited to study them. Are their characteristics (jets, Drell-Yan, heavy flavor) consistent with the structure of $\mathcal{P}$ deduced from SDE? Do we see a component with both $\mathcal{P}$'s apparently behaving as a single hard object, e.g. with $\mathcal{P}\mathcal{P} \rightarrow b\bar{b}$ and nothing else? The approximate mass limit (for x_{min} = 0.95) is 100 GeV for the central system at the Tevatron. Of course, higher masses are produced but with increased background. To study DPE, one ideally would like to insert Roman Pot Spectrometers on both downstream arms and to measure both "quasi-elastic" ($x > 0.95$) proton and antiproton. This should be possible in Run II, but it would require the construction of a new "spool piece" insertion for the machine. With a single Roman Pot Spectrometer in Run IB we can do tests to see if we can isolate the DPE reaction on the basis of a single high-x $\bar{p}$ and rapidity gaps at small angles on both sides. After that we will be in a better position to judge whether the other arm is necessary.

2 Forward Spectrometer

2.1 General considerations

Inelastic diffractive scattering is characterized by an (anti)proton with high Feynman-x, typically $x > 0.95$. This (anti)proton stays close to the beam until the first dipoles begin deflecting it away. It can be detected at a suitable position downstream in small detectors placed in vacuum insertions or "Roman Pots", which can be moved close to the circulating beam during a run. For most of the physics we propose to do it is necessary to detect this quasi-elastically scattered (anti)proton. Measurement of the momentum and angle of the (anti)proton yields both M^2 and t, i.e. it "tags the pomeron", and allows us to boost properly to the pomeron-proton rest frame. Studying event structures versus M, the $\mathcal{P}$-p c.m.s. collision energy, is one of our main goals. Knowledge of t, equivalent to the squared mass of the virtual pomeron, also enables us to study the t-dependence of the pomeron structure.

One can describe the trajectories of the quasi-elastically scattered protons from their point of origin $(x, y, z) = (0,0,0)$ to the place at which they are detected (x', y', z') using transfer matrices. Ignoring for a moment the (small) effects introduced by the electrostatic beam separators, there is no coupling between the x and y motions, which keeps the problem simple.

On the outgoing antiproton arm there is a so-called "spool piece" 56.54 m from the interaction point, where Roman Pots can be mounted. This is at the far end of the 63-foot long A48 dipole. On the other side of B0 (outgoing proton) there may be a possibility of using a short spool piece for a "single pot detector" after the B11 dipole, but not for a doublet or triplet of detectors, which one would like to have in order to define well a trajectory. However, we would only need both arms for "double-tag" experiments on Double Pomeron Exchange, in which case having a scaled-down arm on one side should be sufficient. The detector on the outgoing antiproton side is adequate for the single diffractive excitation studies, and this is all we are proposing for Run IB. There is a space of 6.5 ft (2.07 m) in which we will mount a triplet of detectors to measure a precise straight line track with redundancy. A top view of the arrangement is shown in Fig. 1. Three identical pipe sections support the pots in expandable bellows, on the inside of the ring. They can be moved in together to within about 1 cm of the beam.

The transfer matrices from $z = 0$ to the detectors are as follows [8]: Let $X = (x, \theta_x, \Delta p/p)$ and $Y = (y, \theta_y)$. Then $X' = MX$ and $Y' = NY$, where (measuring length in meters)

$$M = \begin{pmatrix} -1.649 & 9.279 & 0.230 \\ -0.005 & 0.311 & 0.115 \\ 0 & 0 & 1 \end{pmatrix}$$

$$N = \begin{pmatrix} -2.780 & 2.413 \\ -0.101 & -0.272 \end{pmatrix}$$

If the interactions producing the high-x protons take place at x=y=0, then a look-up table can output θ' and $\Delta p/p$, and hence (t, M^2). Thus we could set up a trigger on a mass and t-range, and tune the rate to be compatible with parallel running. Of course, since we are 57 m downstream of the detector, the signal would not be prompt at the trigger electronics; it will arrive about 400 nsec late relative to prompt signals from B0 and this delay must be taken into account in designing a diffractive trigger.

We are interested in the variables $|t|$ and Feynman-x in the range $0 < |t| < 5\ GeV^2$ and $0.01 < 1 - x < 0.1$. These variables can be expressed in terms of track parameters at B0 as follows (p_0 is the beam momentum):

$$\Delta p/p = 1 - x \qquad\qquad |t| = p^2\theta^2 = (xp_0)^2\theta^2$$

$$|t|^{1/2} = xp_0\theta \qquad\qquad \theta = \frac{|t|^{1/2}}{xp_0}$$

$$|t| = |t|_\mathrm{x} + |t|_\mathrm{y} = (xp_0)^2\theta_\mathrm{x}^2 + (xp_0)^2\theta_\mathrm{y}^2$$

The track variables at the Roman Pot location are x$'$, y$'$, θ'_x and θ'_y. In order to get an understanding of the kinematics and the acceptance, let us consider the case of x=y=0 at B0, since a sub-millimeter x- or y-displacement at B0 has small effect on these variables. We then observe the following:

In the vertical y-direction we get

$$\mathrm{y}' = 2.413\,\theta_\mathrm{y} \qquad\qquad \theta'_\mathrm{y} = -0.272\,\theta_\mathrm{y}$$

Since the maximum θ_y we are interested in is $\frac{\sqrt{5}}{0.9\times 900} = 0.003$, we expect $\mathrm{y}'_{max} = 7\,mm$ and $\theta'_{\mathrm{y},max} = 0.002$, which is a 2 mm displacement over 1 m. Therefore a $\pm 1\,cm$ detector system with a 1 m lever arm will have full acceptance in the vertical direction.

In the horizontal x-direction the variables x$'$ and θ'_X can be used to calculate the Feynman-x and the x-component of $|t|$, $|t|_X$. From the matrix equations above we get

$$x' = 9.279\,\theta_X + 0.230(1-x)$$

$$\theta'_X = 0.311\,\theta_X + 0.115(1-x)$$

These equations yield

$$1-x = \frac{1}{0.230}(x' - \frac{9.279\sqrt{|t|_X}}{xp_0}) = \frac{1}{0.115}(\theta'_X - \frac{0.311\sqrt{|t|_X}}{xp_0})$$

Using the approximation of $x \approx 1$ on the right hand side, $(1-x)$ is linear in $\sqrt{|t|_X}$. Fig. 2 shows the roman pot acceptance region in the $(1-x)$ versus $\sqrt{|t|_X}$ plane in this approximation for a detector system with a lever arm of 1 meter. We see that for $(1-x) \approx 0.5$ the acceptance region is in the range $0 < |t| < 5\,GeV^2$ for a detector covering the region $10 < x' < 35\,mm$.

The variables t and $(1-x)$ are given in terms of x$'$ and θ' as follows:

$$1-x = 9.320\,\theta'_X - 0.312\,x'$$

$$\sqrt{|t|_X} = x\frac{p_0}{8.657}(x' - 2\theta'_X)$$

These equations show that:

- For $t = 0$ we have $x' = 2\theta'_X$.
- $(1-x)$ is given mainly by θ'_X rather than by x$'$ (see Fig. 2), so that it is possible to set-up a hard-wired trigger to select a given range of $(1-x)$ irrespective of $|t|_X$.
- For a given θ'_X or $(1-x)$, the $|t|$-value is given mainly by the value of x$'$, so that it is possible to trigger on high t-values, while maintaining approximately the same $(1-x)$, by pulling the detectors away from the beam (see again Fig. 2).

The x and t resolutions can be calculated from the last two equations. Approximately, we have:

$$\delta(1-x) = \frac{9.320}{\text{lever arm}}\delta(\Delta x') \approx 0.01\,\delta(\Delta x')(mm)$$

$$\delta\sqrt{|t|} \approx 100\,\delta(x' - 2\theta'_X) \approx 0.1\delta x'\,(mm)$$

where $\Delta x'$ is the x-displacement of the track in the two outermost detectors (over the 1 m lever arm).

We note that $\delta x'$ dominates the uncertainty in t, since the measurement of x' depends on knowledge of the beam position, which can be known to an accuracy of ≈ 0.5 mm, a value to be compared with the accuracy in $\Delta x'$ over the 1 m lever arm of the detector system, which is 0.2mm for detectors with intrinsic space resolution of 150 μ. Thus, we expect approximately $\delta(1-x) = 0.002$ and $\delta|t| = 0.1\sqrt{|t|}$, the latter dominated by the beam position uncertainty. These resolutions are adequate for the proposed measurements.

2.2 The scintillating fiber tracker

The scintillating fiber tracker consists of 40 ribbons (per pot, for each of 3 pots) of KURARAY SCSF81 fibers being read out by a HAMAMATU H4120 256-channel multi anode PMT (MAPMT). Each fiber is 0.833 mm $\times$ 0.833 mm square, 20 cm long, and has a scintillating core of 0.800 $\times$ 0.800 mm. One ribbon is made of 4 such fibers. On the detecting side, the 4 fibers of a ribbon are arranged in-line (one behind the other along the beam direction) to increase the path length of the particle in the scintillator, while on the phototube side the ribbon is rearranged into a square to fit the shape of the anode of the MAPMT.

The tracker has two detecting layers, or one superlayer, in each of x and y views. In each of the detecting layers, 20 ribbons are placed parallel to each other with a spacing equal to one third of the scintillating core width (see Fig. 3). The second layer is displaced from the first by two thirds of the scintillating core width. Thus, each ribbon can be divided into three regions: one in which two layers do not overlap with each other, and two in which a ribbon in one a layer overlaps with one in the other layer. The detecting region of width 21.87 mm is thus divided into 79 cells of 0.267 mm. The expected spatial resolution for perfect performance is thus 77.0 μm.

The superlayer structure is made of an aluminum fiber holder with aluminized mylar spacers. Fig. 3 shows details. In each layer, the gaps between ribbons are maintained by the aluminized mylar spacers, guided by grooves on the aluminum support structure.

The scintillation light from the 40 ribbons is converted to electrical signals by a multi-anode PMT. The PMT has ten fine mesh dynodes with a built-in voltage supplier and 256 individual 2.34 mm square anodes. We use 200 of these anodes assigning 5 channels to each of the 40 ribbons, using a home-made external connector board. This multi-anode PMT enables the tracker to be a compact system.

The signals will be digitized, possibly locally, and sent upstairs for processing; we do not need to read out pulse-heights or times.

2.2.1 Experimental tests

A test of the characteristics of the tracker was made using a 1 GeV π^- beam at the KEK PS. Three identical trackers were placed along the beam direction. We call these trackers Tr1, Tr2, Tr3 from up- to down-stream along the beam. The three trackers were sandwiched by 17 mm wide trigger scintillators. We defined a track with Tr1 and Tr3, and examined the residual of Tr2.

A hit cell of each tracker was identified by a signal in a LeCroy 1885F FASTBUS ADC. To avoid misidentification caused by noise, we considered the entire data for the identification of each hit cell.

Out of 29328 events recorded, we only had two events with no signal. We define the efficiency as the fraction of events in which the residual is smaller than 3-σ, defined from the whole sample. The efficiency over all cells is 98.1%.

Fig. 4 shows the distribution of residuals over all positions in Tr2 and the resolution versus position. The resolution is 134 μm on average. We believe the larger value of the resolution compared with the expected spatial resolution of 77 μm is due to the misalignment of fiber ribbons, caused by a twisting force applied to the fiber bundles just outside of the detector. This problem could be easily solved in the production of the real detector.

The three detectors in the antiproton arm will be mounted on precision mechanics with remote controlled motors that can move the detectors horizontally towards the beam. An automatic stop when the rate in the backing scintillator exceeds a predetermined level would prevent the detector from disturbing the beam significantly. Note that we are not as critical on the issue of "getting close to the beam" as our previous experiment measuring elastic scattering and low-mass diffraction. The relatively large momentum difference between the beam and the scattered antiproton gives a larger spatial separation. Also, we will take data with the standard low-beta optics.

2.3 Trigger scintillators

The fiber tracking arm, with its three 22mm $\times$ 22mm fiducial areas, will be augmented with up to 6 small scintillation counters. These can be used to provide a prompt coincidence defining the fiducial area, and will have sufficiently good timing that we can discriminate (if it be necessary) against wrong-direction background. We will also have the capability of selecting single minimum ionizing particles. These will require 6 ADC and 6 TDC channels.

3 Trigger, Cross-Sections and Rates

Single diffractive excitation has a very large total cross section, of order 9.5 mb at $\sqrt{s} = 1800$ GeV [6]. However most of the cross section is for low mass (the cross section drops like M^{-2}) and low $\mid t \mid$ (the t-dependence is about $e^{\sim 7t}$ with t in GeV^2). We do not have acceptance in the low (t, M^2) region (see Fig. 2), but this region is not as interesting as the higher mass region where hard phenomena appear. We therefore aim to select at the first level trigger a region of the (t, M^2) plane such as $\sim 200 < M < 300\ GeV$ and $\sim 0.25 < |t| < 5\ GeV^2$ (approximately the full range). This corresponds to tracks traversing the pot detectors with angles around 2-4 mr, to be compared with about 0.07 mr resolution (100 μm over 1500 mm). We can thus define a coincidence matrix (x_1, x_2, x_3) with allowed combinations for desired (M, t) values, and this can be done with a look-up table which is very fast on the time scale of level 1. The main component of the delay in forming a level 1 trigger is the flight time of the antiproton, 180 ns from the interaction, and sending the signals back to the control room, approximately another 300 ns. We believe this delay is acceptable. The coincidence matrix should be located in the "trigger room" next door to the control room for accessibility. The single yes/no output of the pot coincidence matrix can, if required, be VETOed by a signal of energy (or E_T) above a low threshold in the same-side microplug, described in the next section. Although there are no empty FRED Level 1 inputs at present, we believe it will be possible for the fall running to make one available, evaluating the priorities of the existing assignments. For example one may ask : "Do we still need the BBC coincidence as a level 1 input?"

We are also interested in all data taken with the pot spectrometer operational and used as a diffractive tagger, whether or not it provided a trigger. For example, we have already mentioned our search for rapidity gaps in W and di-jet events. We will be able to similarly search for diffractively scattered antiprotons for all topics studied by CDF. Therefore we are not totally dependent on the forward spectrometer trigger, even though we do consider it important.

4 MicroPlug Calorimeters (Run IB)

In addition to measuring the quasi-elastic antiproton, the small angle region around both beam pipes is important for the single diffraction measurements. The microplug calorimeters were proposed in 1991 [9] to extend the rapidity coverage of the present calorimeters from $4.2 \leq \eta \leq 5.4$. They have several important applications in the context of this proposal. The most important is probably the furnishing of a rapidity gap signal on the downstream antiproton (pot) side. This is similar to what might be provided by a veto on BBC counters, but the latter have the disadvantage that they count very low energy particles from the calorimeters, nuclear fragments etc; what is needed is a device to veto on hadrons above a GeV or so. Rapidity gaps as defined by the extended calorimetry (microplugs + FEM/FHA) can be correlated with the high-x antiproton signal both to clean up the signal and to understand the relation between studies using gaps and studies using high-x antiprotons. An example of how the microplugs can be used to improve the signal to background ratio in rapidity gap studies (no high-x antiproton required) is given in Fig. 6. This figure shows the distribution of the maximum pseudorapidity tower in an event, η_{max}, for both diffractive and non-diffractive events obtained by a Monte Carlo simulation of W-production. For diffractive W, η_{max} is relatively small because there is a rapidity gap to the right. For non-diffractive W, η_{max} tends to be close to the edge of the calorimeter, which is at η=4.2 in the present detector, and at $\eta = 5.4$ for the microplug case with a corresponding reduction in background.

The calorimeter on the downstream proton side is mainly used for extending the rapidity coverage of calorimetry for the high mass state, of which we want to detect as much as possible, including very forward particles. For example one can calculate, using calorimetric energy vectors, the total effective mass of the hadronic system. The resolution will not be very good but there should be a correlation with the missing mass to the antiproton, which may be a useful tool for background studies. In general this calorimeter helps also in studying the topology of the excited system. It allows the measurement of jets to extend about one unit of rapidity further, particularly useful for the "two-forward-jet" physics probing very low-x phenomena.

Another possible use of this p-side calorimeter is to look for double pomeron exchange events by requiring a calorimetric rapidity gap also on this side.

The microplugs are octagonal "cylinders" which fit inside the hole in the FEM calorimeter, with "radius" from 2.25″ to 5.62″ and total length 22″ (see Fig. 5). The calorimeters are 22 X_0 and 0.7 λ_0 in length; they are basically electromagnetic calorimeters but have some efficiency for hadrons also. The technique is lead-scintillator sandwich, reading out the scintillating tiles with wavelength shifting fibers. Eight photomultipliers read the eight ϕ octants. The device also contains a shower maximum detector made of scintillating bars/ wls fibers/ MAPMT, but we do not propose to instrument it now. The shower maximum detector design and performance are discussed in detail in Ref. [10].

The microplugs are already constructed and a four-tower model was tested in a beam [11]. Of course the device is close to 100% efficient for energetic electrons and photons, and the energy resolution is

$$\sigma(E)/E = 22.5\%/\sqrt{E} \oplus 0.2\%.$$

The calorimeter is linear for electrons from 30 - 150 GeV at the 1% level. Muons are detected with close to 100% efficiency, so we can also count charged hadrons.

Our support requirements are minimal; the basic hardware already exists. We ask for help from CDF in mounting the microplugs inside the FEM calorimeters, and surveying them. They require 8 HV and 8 signal cables per side, plus ADC channels and a small amount of logic for inclusion in the trigger (as an option).

5 MiniPlug Calorimeters (Run II)

In the era of the Plug Upgrade, Run II and beyond, presently approved calorimetry extends only down to 3^o ($\eta = 3.6$), the half angle of the conical edge of the upgrade calorimeter. The beam rapidity is 7.6, so ignoring differences between y and η there are 4 units practically uninstrumented. A very small (by CDF standards) calorimeter, the "miniplug" can fill a substantial part of this hole, down to 0.5^o ($\eta = 5.4$). The motivation for the miniplugs is similar to that previously discussed for the microplugs, only more so, because they are larger. The new plug upgrade calorimeter will give us excellent calorimetry down to nearly 3^o, a very large angle by our standards, making the miniplugs crucial for all the forward physics in Run II.

The proposed miniplug calorimeters can be positioned as shown in Fig. 7 between the back-plate of the plug and the front of the coil of the muon toroid. This allows a thickness of only $\sim 1\ m$, but that is sufficient for about 4 interaction lengths (instrumented). Nearly four more interaction lengths could be added but only out to a radius of 32 cm, by extending the calorimeter into hole in the muon toroid. We do not propose to do this, as the gain is marginal. Each of the two miniplugs (one per end) is therefore approximately a cylinder of outer radius 50 cm (cf 20.8 cm for the inner edge of the plug), inner radius of 2.5 cm (fitting around the beam pipe) and length 1 m. We are considering two technologies for the miniplugs, either of which appears to be well able to meet our specifications. One uses high pressure gas in close-packed steel tubes, approximately parallel to the particles. A steel rod along the axis of each tube acts as an anode, the wall is the cathode. With about 100 atm of Argon-methane or Argon-CO_2 and an applied voltage of typically 1.5 kV (gap = 2 mm) this is a zero gain ionization chamber calorimeter. The other solution is to use a "shish-kebab" design (PAD, for *Pixel Array Detector*): alternate layers of lead plates and liquid scintillator are "skewered" through with wavelength-shifting fibers (pointing along the beam direction), with spacing between fibers of 1 cm in the plane transverse to the beam. The light from these fibers is collected at the back face of the calorimeter by multi-anode PMT's. The design and features of these two calorimeters are described in more detail below.

We expect to have all the relevant information in hand to enable a decision between these two alternative techniques to be made by Fall 1995. In any case, these miniplugs are for Run II when the Plug Upgrade is installed, presently foreseen for 1998. For the first few months of running with the Roman Pot Spectrometer, in Fall 1995, we wish to use the existing "Microplugs".

5.1 High Pressure Gas Miniplug

We now describe briefly the high-pressure gas-ionization tubes option for the miniplug. Two calorimeters based on this technique, hadronic [12] [13] and electromagnetic [14], have been recently constructed and tested by a Rockefeller-FNAL group. The calorimeters consist of steel tubes filled with 95% Argon + 5% methane gas mixture at 100 atm. A thick steel rod in the tube center is held at a voltage of about 1.5 kV and collects the primary charge (there is no charge amplification in the gas). The operation is similar to a liquid argon calorimeter but without the complication of cryogenics. The main advantage of this technique is the enormous radiation resistance of the tubes. Radiation damage tests have shown [15] that the limit, if any, exceeds 1 GRad. At the same time a rather good energy resolution has been obtained with the calorimeters we tested [13][14]:

$$dE/E = (64 \pm 6)\%/\sqrt{E} \oplus 3\%$$

for pions, and

$$dE/E = (32.0 \pm 1.6)\%/\sqrt{E} \oplus (2.9 \pm 0.3)\%$$

for electrons.

The electronic noise is proportional to the square root of the calorimeter volume and with the available amplifiers it is about 6 GeV/m^3. The output signal full width is about 80 ns. The calorimeters have a stable and linear response. The calibration procedure is very simple.

We propose to make the miniplug from two parts (Fig. 8). The central part consists of "wiggler tubes" [14] (slightly bent to avoid 0^o effects) of 9.5 mm outer diameter and 1.4 m length. The tubes are assembled in 18 hexagonal modules with 127 tubes per module. The peripheral part consist of straight 12.7 mm outer diameter, 0.7 m long tubes. The tubes are assembled in 72 hexagonal modules with 61 tubes per module. Both kinds of modules are mechanically robust and independent, and the whole miniplug can be assembled by stacking these modules on a proper supporting table.

The limited length of the miniplug ($\approx 4\lambda$) results in leakage of hadronic shower energy and this deteriorates the hadronic energy resolution at high energies. With this effect and with the above mentioned electronic noise we anticipate a hadronic energy resolution of about 32% for E = 20 GeV, 20% for E = 50 GeV, and 15% for E $\geq$ 200 GeV. The jet resolution should be a little better at high energies. More accurate figures will be obtained by Monte Carlo simulations. The transverse segmentation of the miniplug is good enough to measure transverse energy with the same accuracy as the total energy. At the same time the proposed design allows one to isolate and measure with good accuracy individual EM showers in the central part of the miniplug.

The cost of a central module is about \$5,000 and the cost of a peripheral module is about \$2,200. The total cost of the two miniplugs is about \$300,000 including electronics.

5.2 PAD Miniplug

Another possible technology for the miniplug calorimeters has also been developed by the Rockefeller group, and a proposal for implementing it in CDF was made [16] in 1993. This is called the PAD, for Pixel Array Detector. In the proposal, the PAD consists basically of a tank of liquid scintillator (liquid for simplicity of construction and radiation hardness) containing a stack of 64 lead absorber plates $3/8''$ thick. All the plates have an array (spacing approximately 2 cm) of holes through which pass wavelength shifting fibers. These emerge at the back and go to MAPMTs. A set of extra fibers read out just the back section, after 24 X_o, to tag hadrons. The lead plates are separated by a honeycomb of reflective aluminum to define cells, giving the device excellent granularity. Monte Carlo studies showed that this arrangement should give a position resolution for isolated electrons(pions) of about 2 mm ($\sim$ 1 cm). The good resolution for hadrons is thanks to the π^o component present in most hadron showers. This granularity allows what may be called "calorimetric tracking" [17], providing a large amount of information. This is particularly important in the small angle region because for a given energy particle both p_T and η are very dependent on position.

A PAD prototype was constructed and tested [18] with 5 GeV electrons and 8 GeV pions at the Brookhaven AGS. In this prototype, the lead plates were laminated with reflective aluminum on both sides and **no honeycomb was used to define cells!** The fibers, spaced by 1 cm in x and y (z is the beam direction), were simply grouped in *quartets* defining *cells* of 2 cm $\times$ 2 cm, as shown in Fig. 9. The side view of the prototype is shown in Fig. 10. This design simplifies construction and allows for different ways of grouping the fibers, if so desired.

For the (low) energies of the test beam, we obtained $\sim$ 3 mm position resolution for electrons and 8 mm for pions, in agreement with our Monte Carlo predictions. The energy resolution for electrons was

$$\sigma/E = 23.3\%/\sqrt{E} \oplus 0.4\%.$$

and for pions 66% (note that the prototype was only one interaction length long).

At the present time the PAD calorimeter appears to be eminently suitable for the $0.5^o - 3.0^o$ region.

6 Electronics, DAQ and trigger

6.1 Roman Pots and Microplug for Run IB

There are two microplug calorimeters, one on each side of the detector. Each microplug has 8 photomultiplier output signals. These 16 signals will be routed to the trigger room with RG58 cables and each will be split into two. One of the two signals will be fed into a LeCroy 2249A ADC. Of the remaining signals, the eight from each microplug will be added together with a LeCroy 428F Quad Linear Fan-In/Fan-Out and their sum will be available for the Level 1 trigger and for the 2249A ADC gate. Therefore, we will need a total of two 2249A and two 428F modules for both microplugs.

The three Roman Pot stations output a total of 240 fiber signals from Multi Anode PMT's and 6 scintillator signals from standard PMT's. The 6 PMT signals will be carried to the trigger room with RG58 cables and each will be split into two. One of the two signals will be read out with a LeCroy 2249A ADC and the other with a LeCroy 2228A TDC through a LeCroy 623B Octal Discriminator.

The 240 fiber signals will be carried to the trigger room with RG174 cables and will be fed into LeCroy 4415A Camac Discriminators, which provide two outputs for each input signal. One output will be fed into a Le Croy 2371 Data Register and special combinations of the second output will be fed into LeCroy 2373 Memory Lookup Units (MLU's). The MLU's will be programmed to accept only selected roads through the fiber complex, enabling us to have high efficiency for high mass diffraction while rejecting most beam halo background. The MLU outputs in a logical combination with the scintillator and same side microplug signals (e.g. vetoing sum signals exceeding a few GeV energy) are the diffractive triggers and are fed into Level 1.

In summary, we will need one 2249A ADC, two 623B Discriminators, two 2228A TDC's, fifteen 4415A Camac Discriminators, fifteen 2371 Data Registers a few scalers and a few (the exact number is not known at this time) 2373 Memory Lookup Units for the Roman Pots and the Microplug in Run IB.

6.2 Miniplug for Run II

There will be two miniplug calorimeters, one on each side of the detector. Each will output about 600 signals, through local preamplifiers (for the high pressure gas option) or Multi Anode PMT's (for the PAD option). These outputs will be read out by 8-bit flash ADC's installed in VME crates in the collision hall (one on each side). This type of flash ADC is also used to read other detectors in Run II.

7 Monte Carlo Studies

We have carried out [19] a series of Monte Carlo studies of diffractive events treating the pomeron as if it were a hadron with one of three gluon structure functions: soft, hard and superhard. If ξ is the momentum fraction of the pomeron carried by the parton, in these cases a gluon, then:

$$G(\xi) = 6(1-\xi)^5/\xi$$

$$G(\xi) = 6(1-\xi)$$

$$G(\xi) = \delta(1-\xi)$$

for soft, hard and superhard, respectively. The soft distribution is dominated by low ξ and will be inefficient at producing very high p_T b-quarks or jets compared with the hard distribution. On the other hand, it has a higher gluon density at low ξ and will be more efficient at lower p_T. The hard distribution assumes exactly two gluons sharing the momentum, while the superhard δ -function would hold if and when the pomeron behaves like a single object, e.g. like a photon. In that case we can have reactions like pomeron + quark $\rightarrow$ jet + jet, with no "pomeron spectator fragmentation".

A detailed write up of the Monte Carlo calculations can be found in Ref. [19]. Here we select some highlights.

Consider first $b\bar{b}$ production from gg collisions, as a function of $p_T(b)$. The single diffractive cross-section integrated above 15 GeV is about 100 nb, and is practically the same for all three structure function choices. For lower $p_T(b)$ the soft distribution wins, and for higher $p_T(b)$ the superhard wins, the difference becoming an order of magnitude for $p_T(b)_{min}$ = 50 GeV, at which point the superhard cross section is about 400 pb. These are measurable cross sections, of the order of 5-10% of the total b-production as measured by CDF. For this physics we would not use any special trigger, but simply interrogate the forward spectrometer for all high-p_T b events. The magnitude of the b cross section is not a very powerful discriminant of the pomeron structure function, but the rapidity (η) distribution is. Fig. 11 shows this distribution for the three chosen structure functions, integrated over p_T. The diffractively scattered antiproton is on the left at η = -7.5, adjacent to a rapidity gap of typically 2.5 units; b-quarks from a superhard pomeron tend to be close to the edge of the rapidity gap, while b's from a soft pomeron tend to be far away from it. If one just measures the b in the central region $|\eta| \leq 1.5$, the slope of the η-distribution is very dependent on $G(\xi)$ as can be seen from the figure.

Similar statements can be made for the events with two high p_T jets from the pomeron-proton interaction, which can be studied more easily. The cross section for single diffractive production of two jets with $E_T \geq 16$ GeV is huge, about 30 (or a few) μb integrating over all diffractive masses for hard a pomeron obeying (or not obeying *a la* UA8) the momentum sum rule. To measure it, it might be appropriate to make a special short run (10 hours at a luminosity of $3 \times 10^{30} cm^{-2} s^{-1}$ could give 100,000 events). To study the hard dijet physics in parallel with other CDF running we would select (at level 1) a restricted range of diffractive mass (e.g. 200-250 GeV) and a higher jet threshold (e.g. 50 GeV), which can of course be tuned up to give a rate we can tolerate.

With jets, as with heavy quarks, the angular distributions are very sensitive to the nature of the pomeron. The harder the pomeron, the closer the jets are to the edge of the rapidity gap. As the diffractive mass increases, this tendency becomes clearer. Fig. 12 shows η_{jet} distibutions for two ranges of diffractive mass and for the superhard, hard and soft pomerons. Using both jets we can not only discriminate between different "guesses" for $G(\xi)$, we can actually measure it. Working in the *c.m.* frame of the pomeron-proton collision, the kinematics of the two jets define ξ and x, the fractional momentum of the parton in the proton. Fig. 13 shows a simulation of this procedure using a simple parton level calculation, illustrating the soft and hard structure functions (the superhard is a δ function, too hard to draw!).

Drell-Yan dileptons, W and Z have also been studied by a simple $q\bar{q}$ pomeron Monte Carlo. Obviously their measurement will be a strong test of the presence of quarks in the pomeron, which must be there at some level from simple evolution. Our rapidity gap search in W events puts an upper limit of 2.1% (95% CL) on the fraction produced by single diffraction, implying that the pomeron is not dominated by hard quarks and antiquarks. However this study is sensitive primarily to pomerons with very low $|t|$ and it may be quite different when $\mid t \mid$ increases to values of several GeV^2; this is one thing we will be able to study.

8 Summary and Conclusions

To summarize, the addition to CDF of a triplet of small track detectors 57 m downstream from B0 would enable us to exploit a wide range of additional physics. By tagging the pomeron emitted from the antiproton in diffractive scattering, and studying the pomeron-proton interactions producing high p_T jets, heavy flavors and W/Z, we can measure the parton content of the pomeron (assuming we find that concept to be valid; if not, it will still make the QCD news!). In particular we can do this from $\mid t \mid$ near 0 GeV^2 to $\mid t \mid$ near 6 GeV^2 to test theoretical suggestions that the pomeron changes its nature through this range.

References

[1] Experiment UA8
R.Bonino et al., Phys. Lett. B211 (1988) 239;
A.Brandt et al., Phys.Lett. B297 (1992) 417

[2] A.Donnachie and P.V.Landshoff, Phys. Letters B296 (1992) 227.

[3] T.Devlin, Description of Rapidity Gap Analysis, CDF/ANAL/JET/CDFR/1906 (1993); "Observation of Rapidity Gaps in $\bar{p}p$ Collisions at 1.8 TeV", CDF/PUB/JET/CDFR/2639, PRL (submitted).

[4] A.Bhatti and K.Goulianos, "Rapidity Gap Results From The Forward Dijet Trigger Data of 1992-93", CDF/ANAL/JET/CDFR/2798 (Version 2.0).

[5] P. Draper (D0), talk at Vth Blois Workshop on Diffractive and Elastic Scattering, Brown University, Providence RI, June 1993.

[6] F. Abe et al., "Measurement of $p\bar{p}$ Single Diffraction Dissociation at $\sqrt{s}$=546 and 1800 GeV", Phys. Rev. D50 (1994) 5535.

[7] S.Bagdasarov and K.Goulianos, "Search for Diffractive W Production in $p\bar{p}$ Collisions at $\sqrt{s}$ = 1.8 TeV", CDF/ANAL/JET/CDFR/2921.

[8] John Marriner, private communication.

[9] "Microplug - A proposal ...", G. Apollinari et al., CDF/DOC/CALORIMETRY/CDFR/1450.

[10] "A novel electromagnetic shower maximum position detector", G. Apollinari et al., NIM A324 (1993) 475-481.

[11] "Microplug test-beam results", G. Apollinari et al., CDF/DOC/CALORIMETRY/PUBLIC/1736 (Jan 1992)G.Apollinari et al.)

[12] S.L.Bagdasarov et al., Nucl. Inst. Meth. A351 (1994) 336. "Beam test of a hadron calorimeter made of high pressure gas-ionization tubes."

[13] S.L. Bagdasarov et al., Nucl. Instr. and Meth. A351 (1994) 336.

[14] S.L. Bagdasarov et al., FERMILAB-Pub-95/004, to be submitted to NIM.

[15] L. Demortier et al., to be submitted to NIM.

[16] "Beyond the plug upgrade; PAD: a Pixel Array Detector for the forward region of CDF in run II", S. Bagdasarov and K. Goulianos, CDF 2237.

[17] "Calorimetric Tracking of High Energy Particles", S. Bagdasarov and K. Goulianos, Proceedings of the 4th International Conference on Calorimetry in High Energy Physics, World Scientific (Eds. A. Menzione and A. Scribano), p. 524.

[18] "Test-beam results of a miniplug calorimeter prototype", S. Bagdasarov, K. Goulianos, A. Maghakian and Q.F. Wang, CDF 2867.
"Pixel Array Detector for forward calorimetry", presented at the 5th International Conference on Calorimetry in High Energy Physics, September 25 - October 1 (1994), Brookhaven National Laboratory, Upton, NY, USA.

[19] T.Arisawa, "Heavy quark production by hard diffractive scattering", Rev. Mod. Physics.

Roman Pot Setup

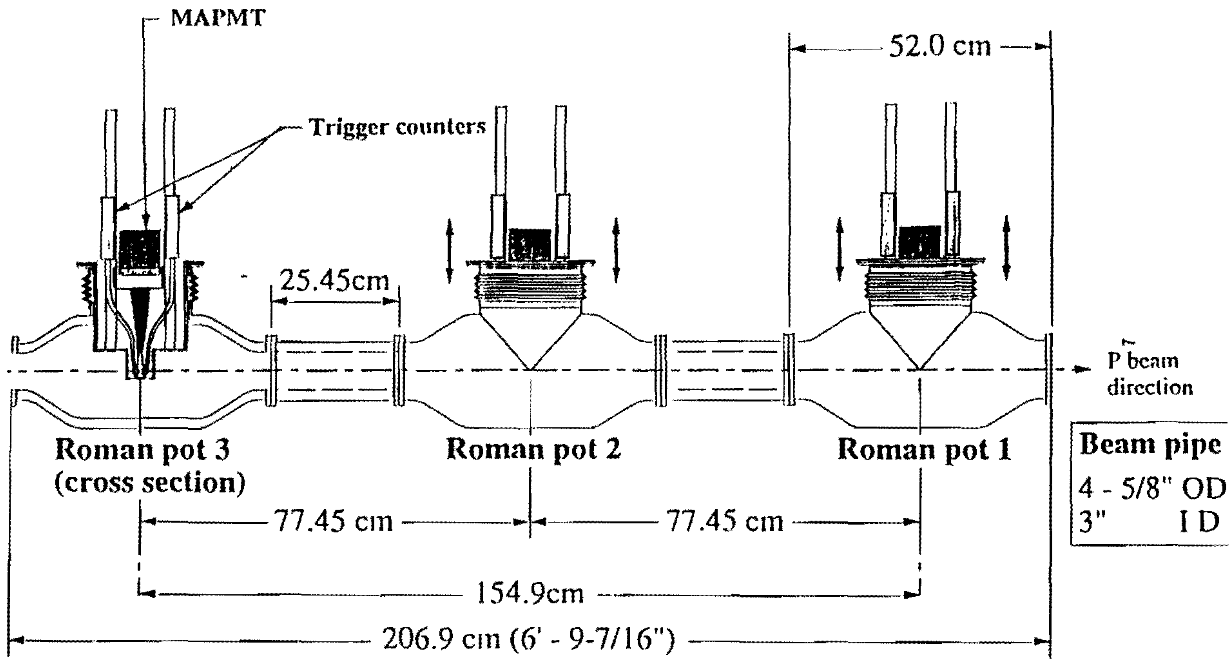

Roman Pot cross-section

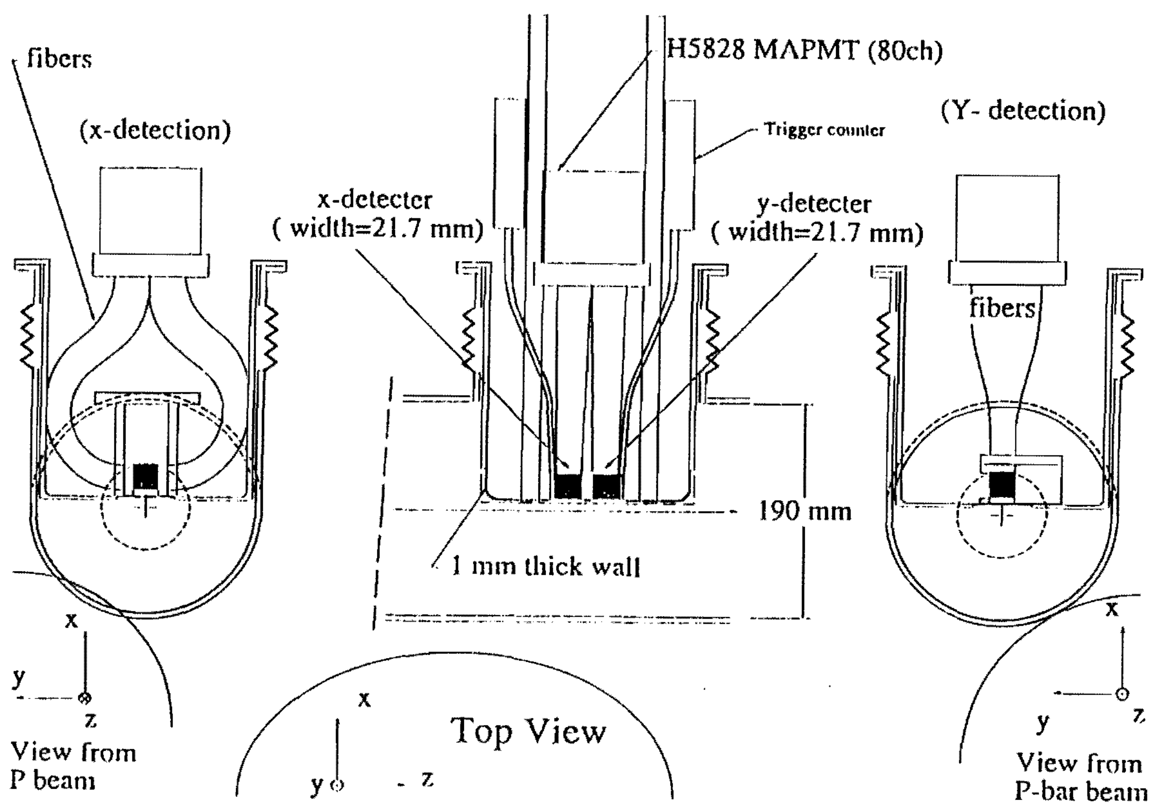

Figure 1: Roman pot arrangement.

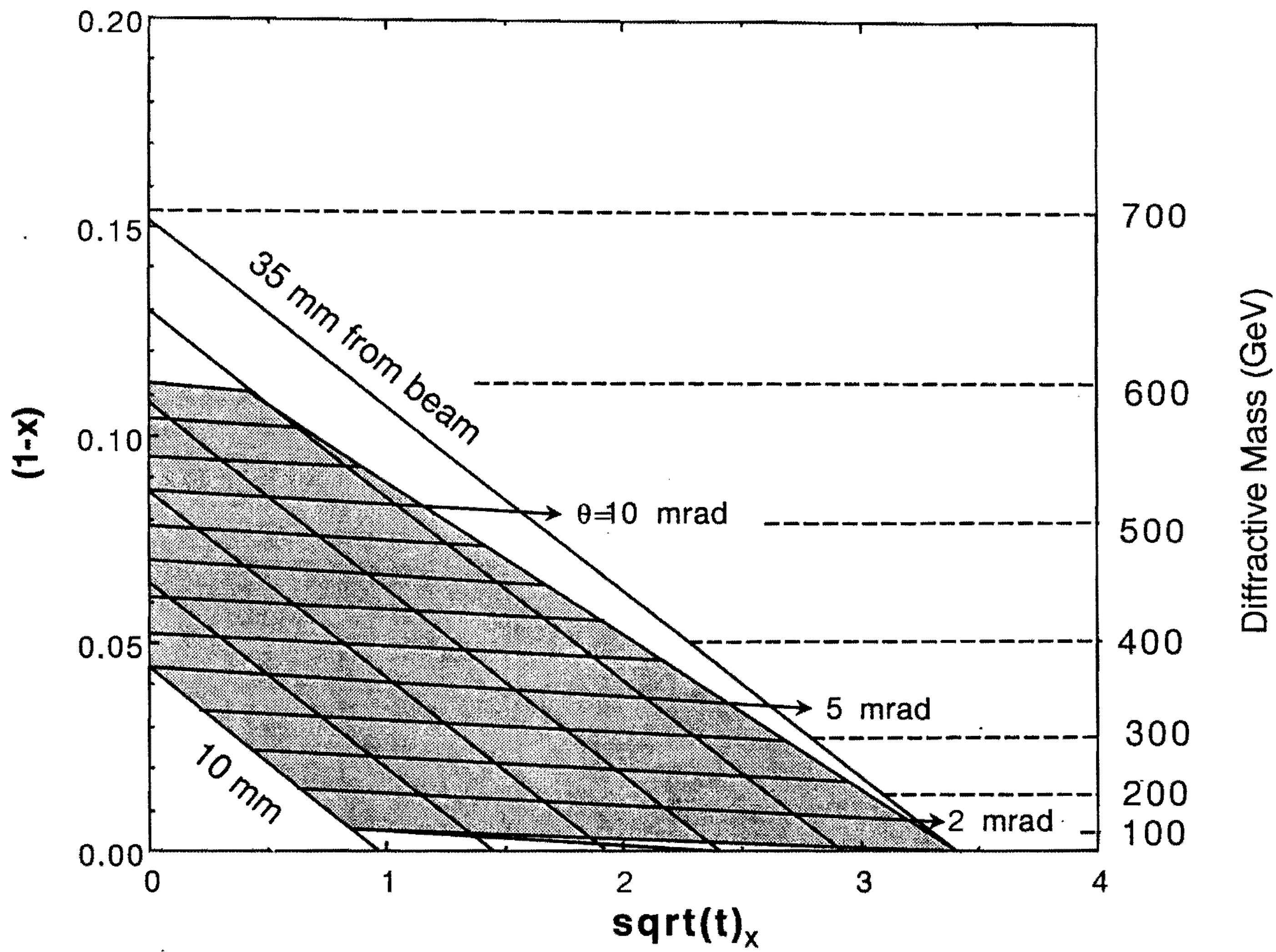

Figure 2: Roman pot acceptance: $(1-x)$ versus $\sqrt{|t|_X}$ as a function of distance from the beam and of the angle θ_X at the roman pot site.

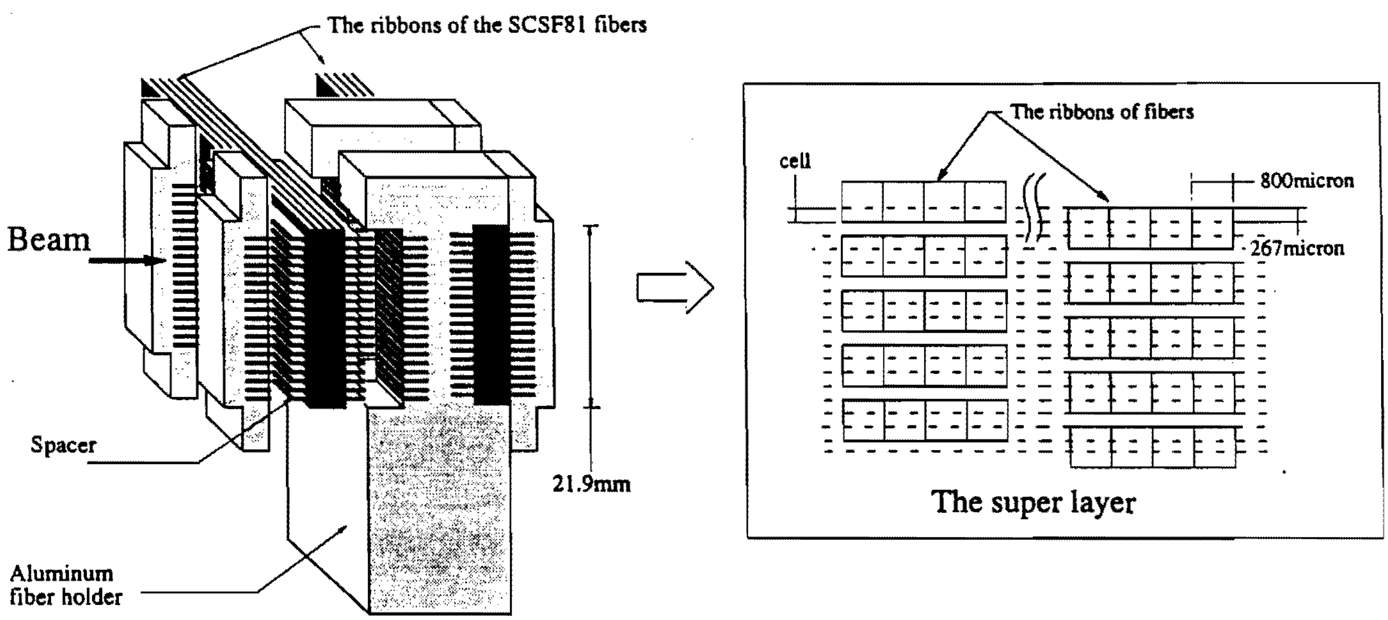

Figure 3: Tracking detector superlayer.

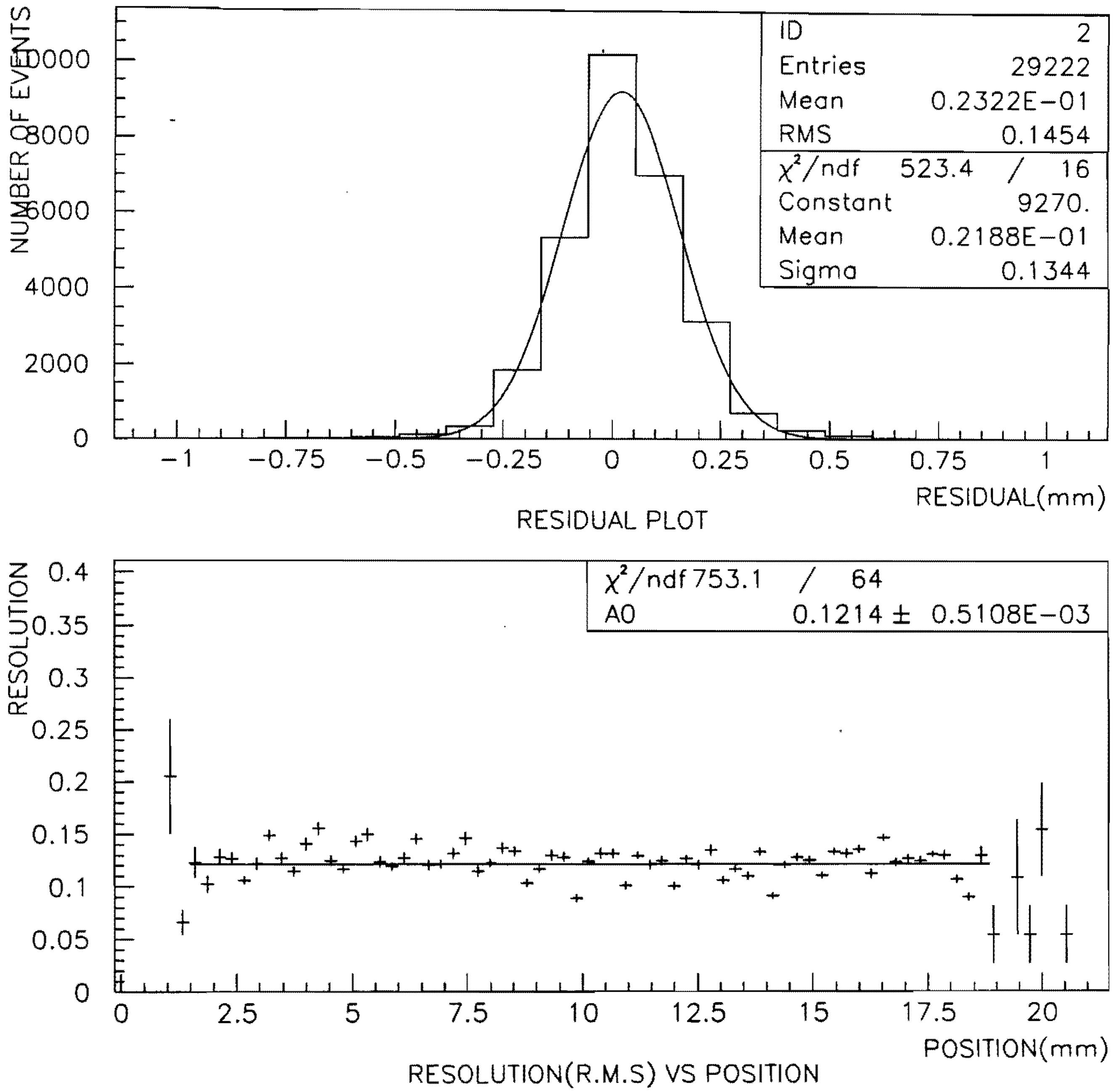

Figure 4: Residuals from tracking detector test (see text).

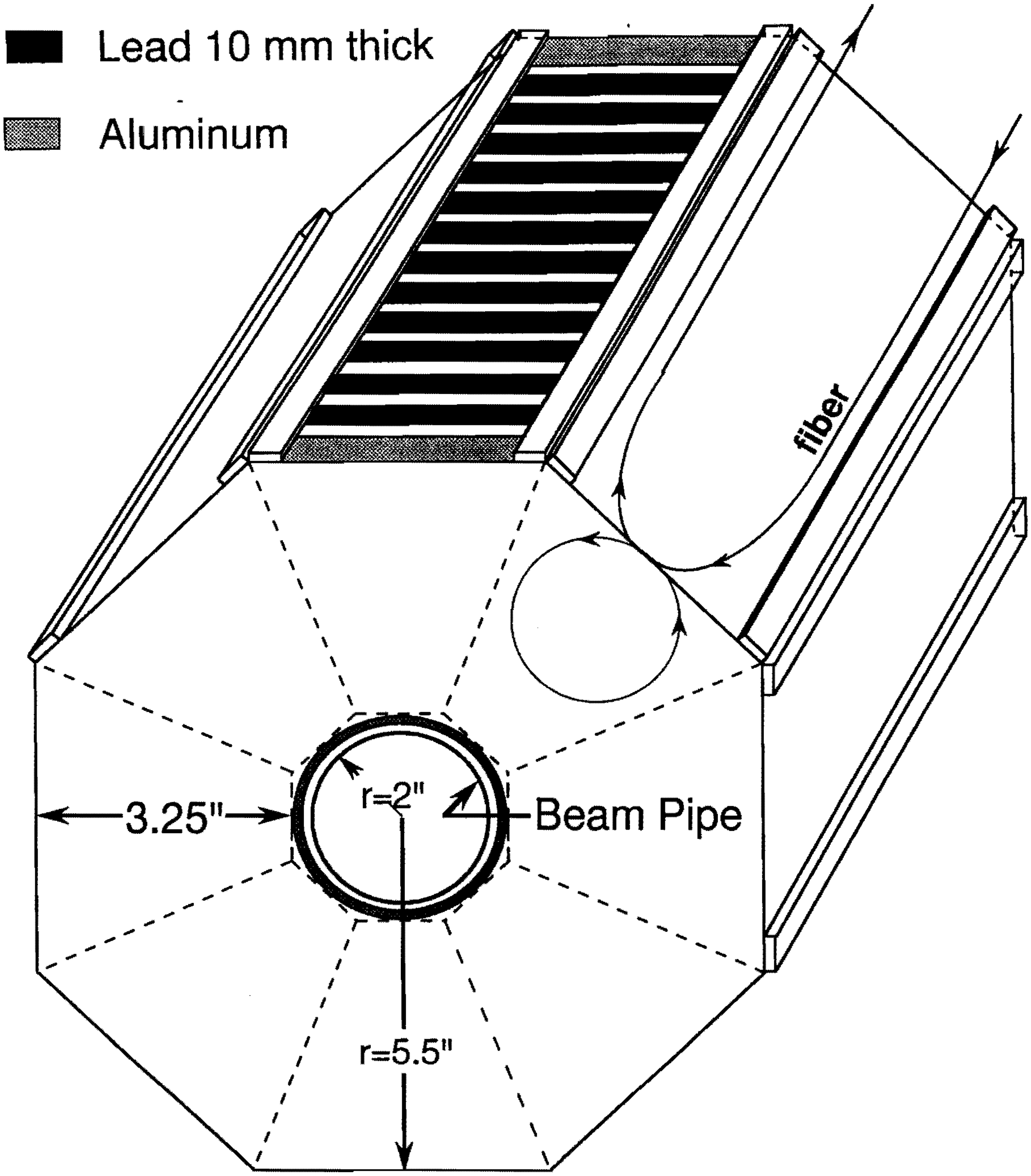

Figure 5: Schematic drawing of the Microplug calorimeter.

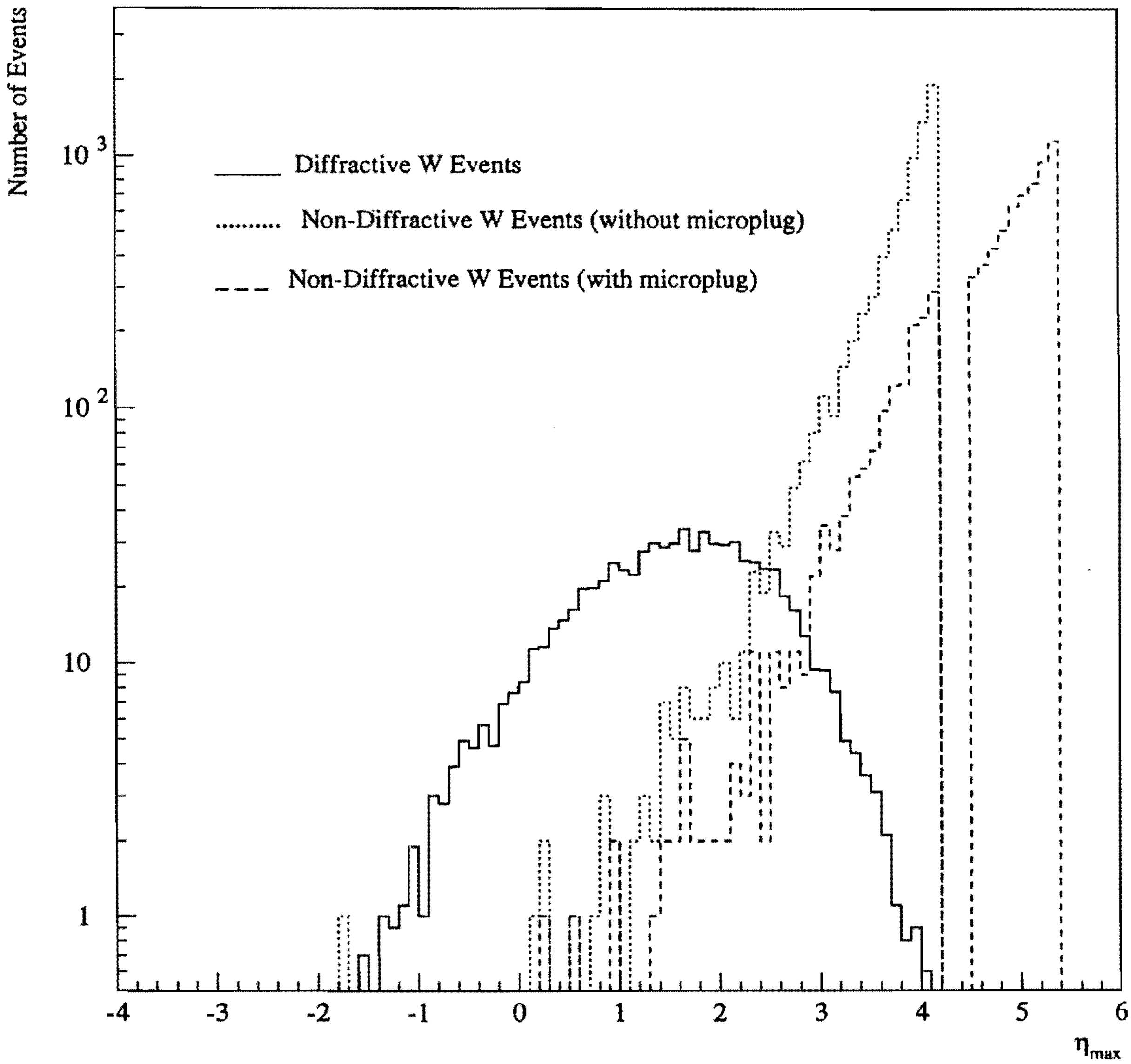

Figure 6: Diffractive and non-diffractive η_{max} distributions for W-production events generated by POMPYT with a hard pomeron structure function.

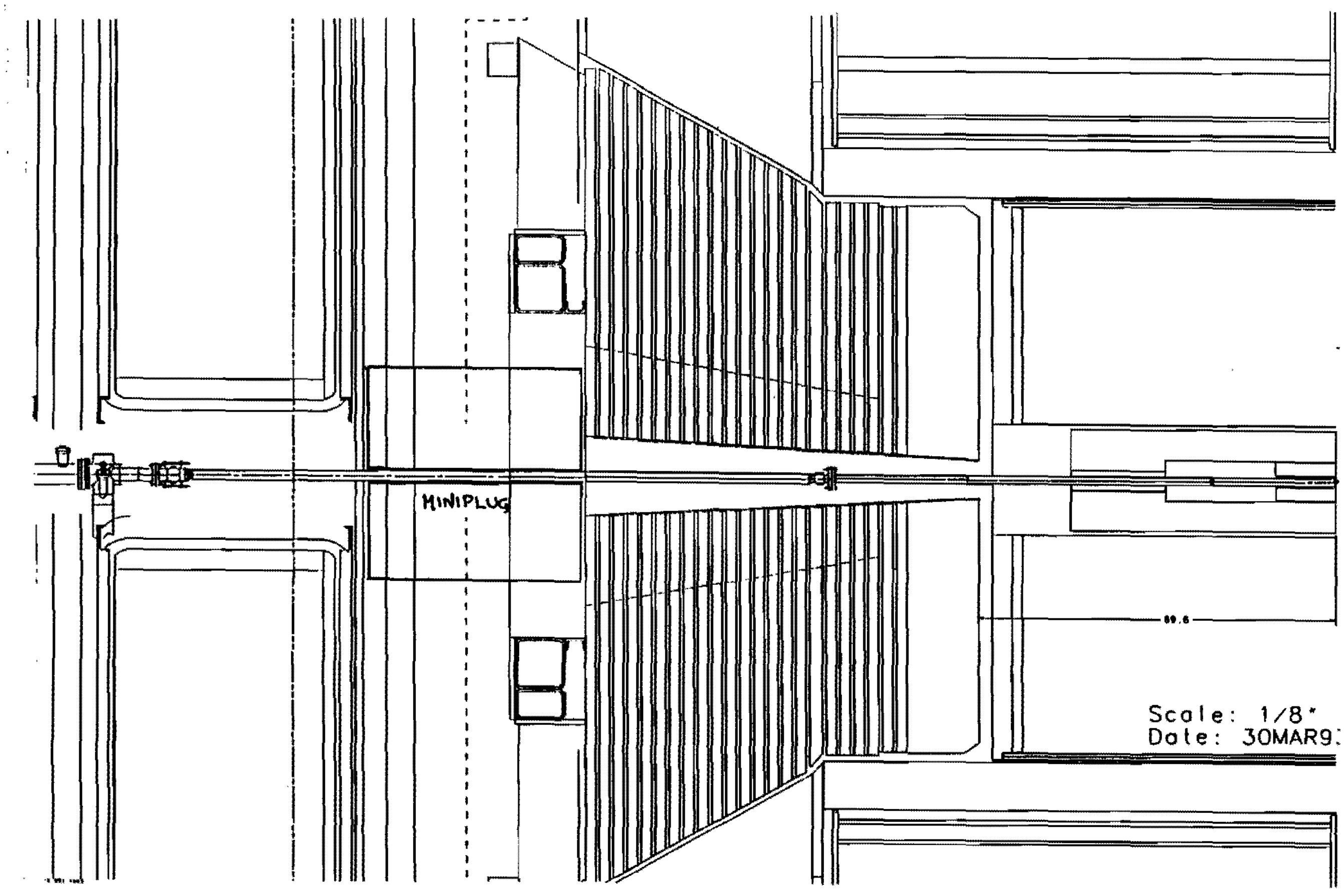

Figure 7: CDF configuration in Run II showing the miniplug position.

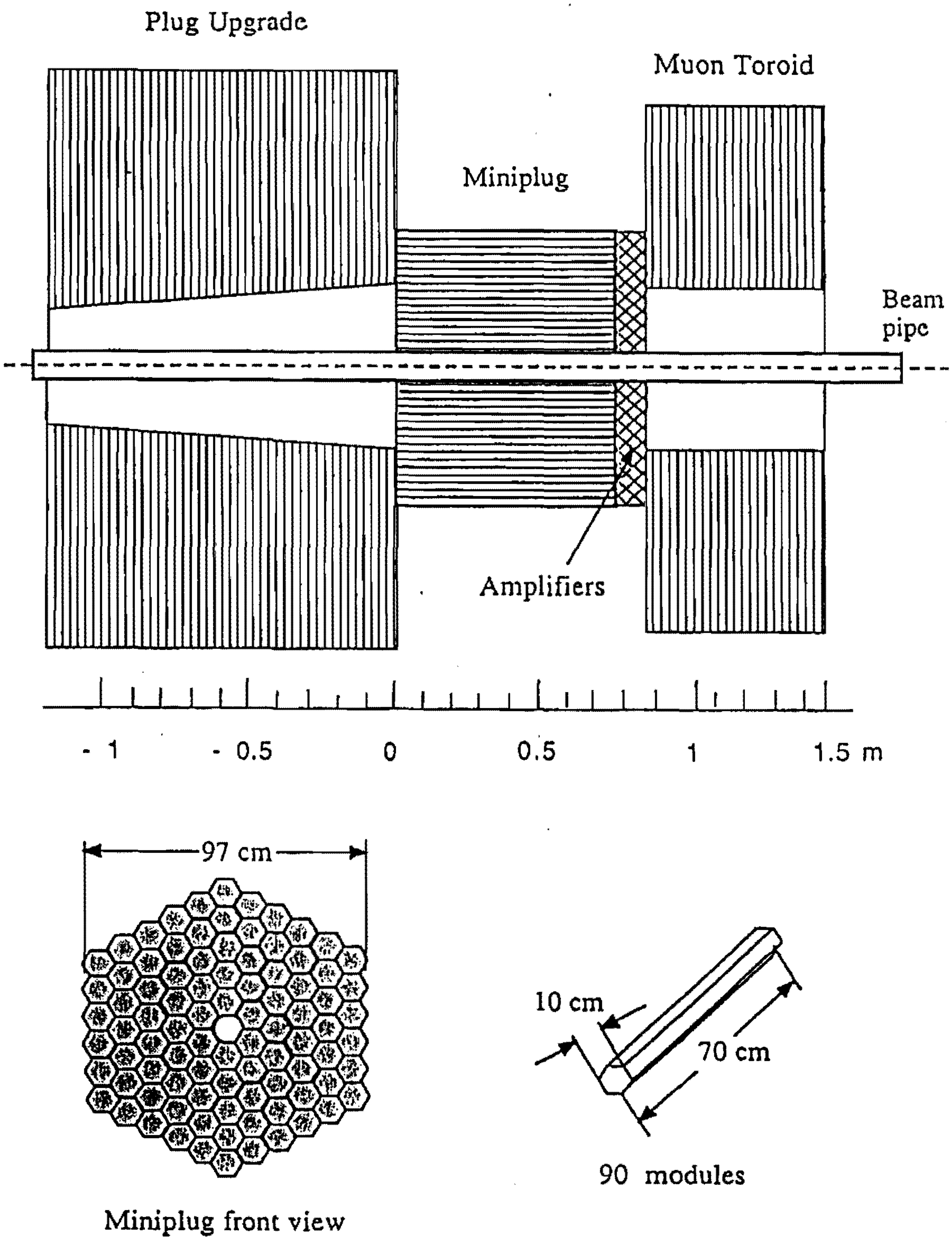

Figure 8: High pressure gas miniplug.

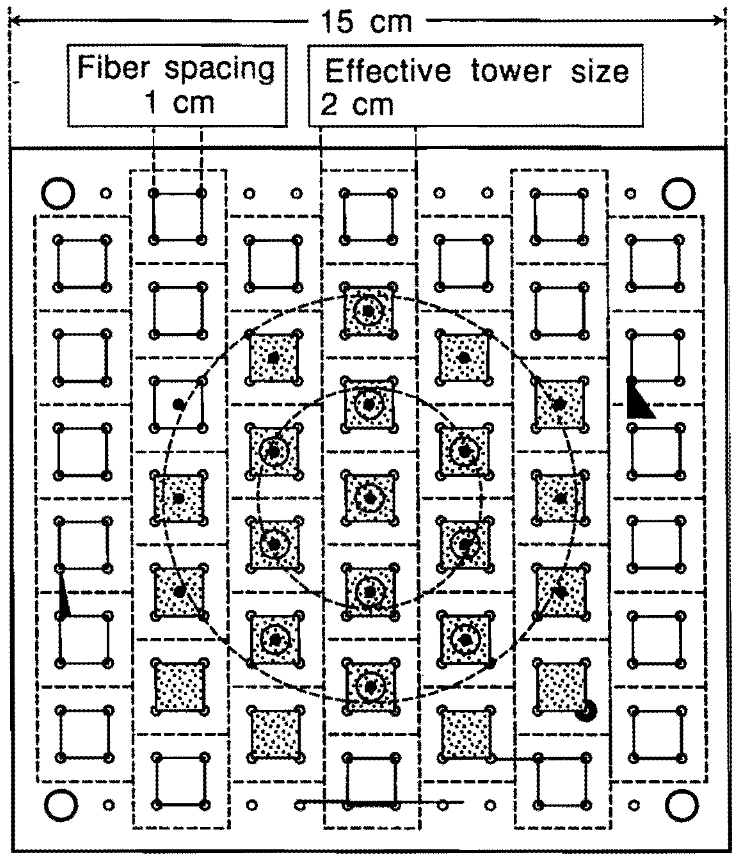

Front view of the PAD prototype calorimeter. Each group of four fibers in a square is read by the same MCPMT channel. The shaded squares and encircled single fibers denote the channels instrumented in the test beam. The beam was directed into the tower at the center.

Figure 9: Front view of PAD miniplug prototype calorimeter.

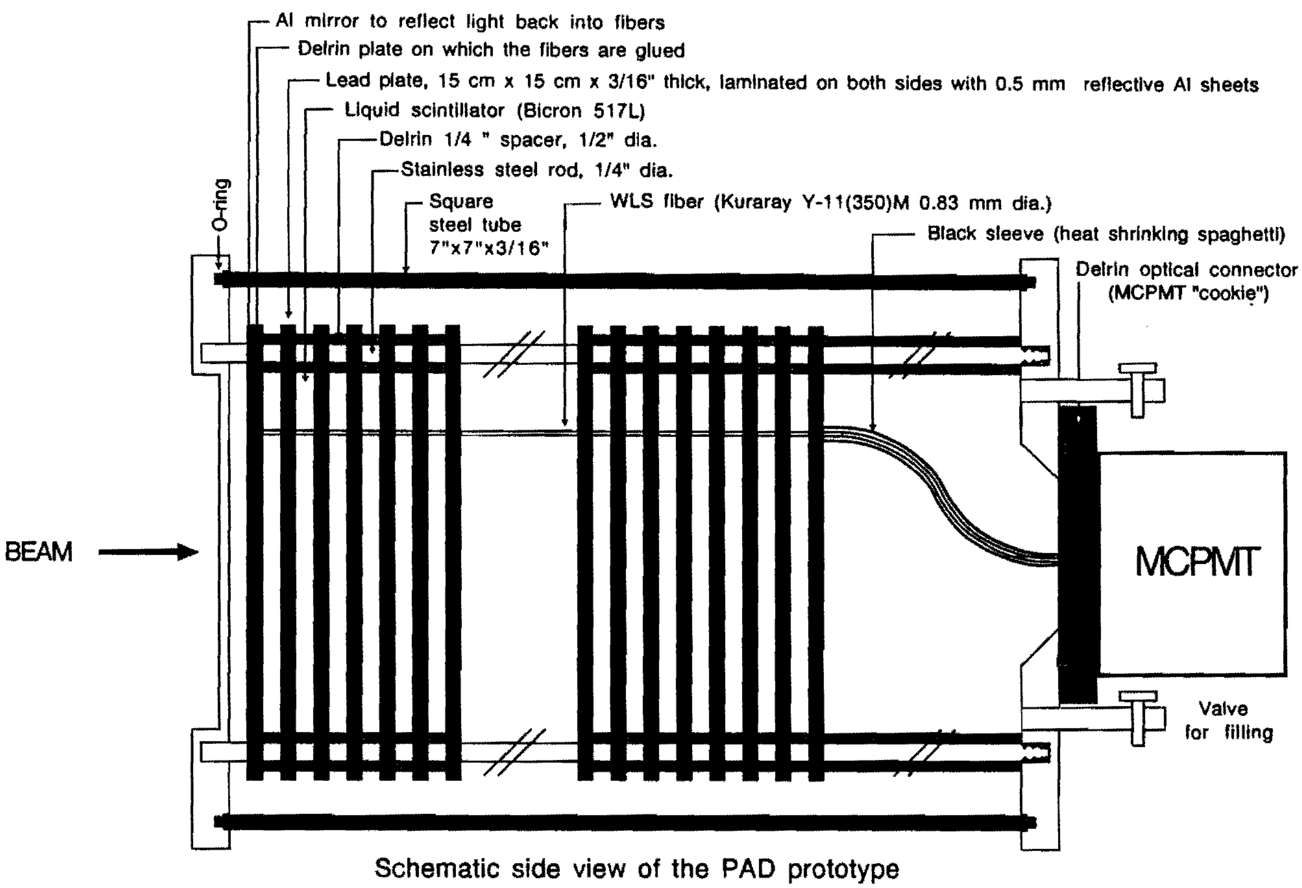

Figure 10: Side view of PAD miniplug prototype calorimeter.

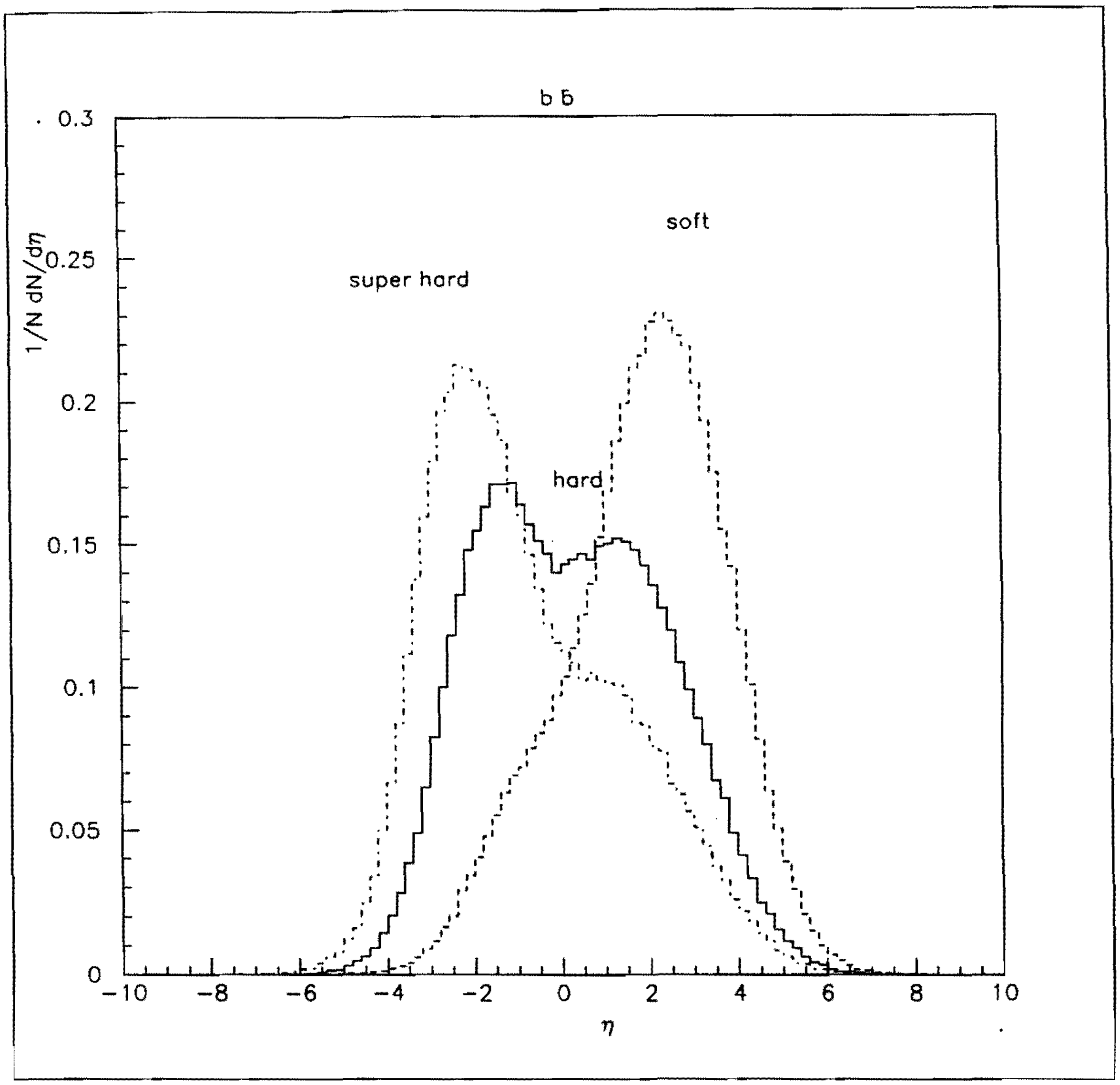

Figure 11: η-distribution of b's (integrated over p_T) for superhard, hard and soft pomerons.

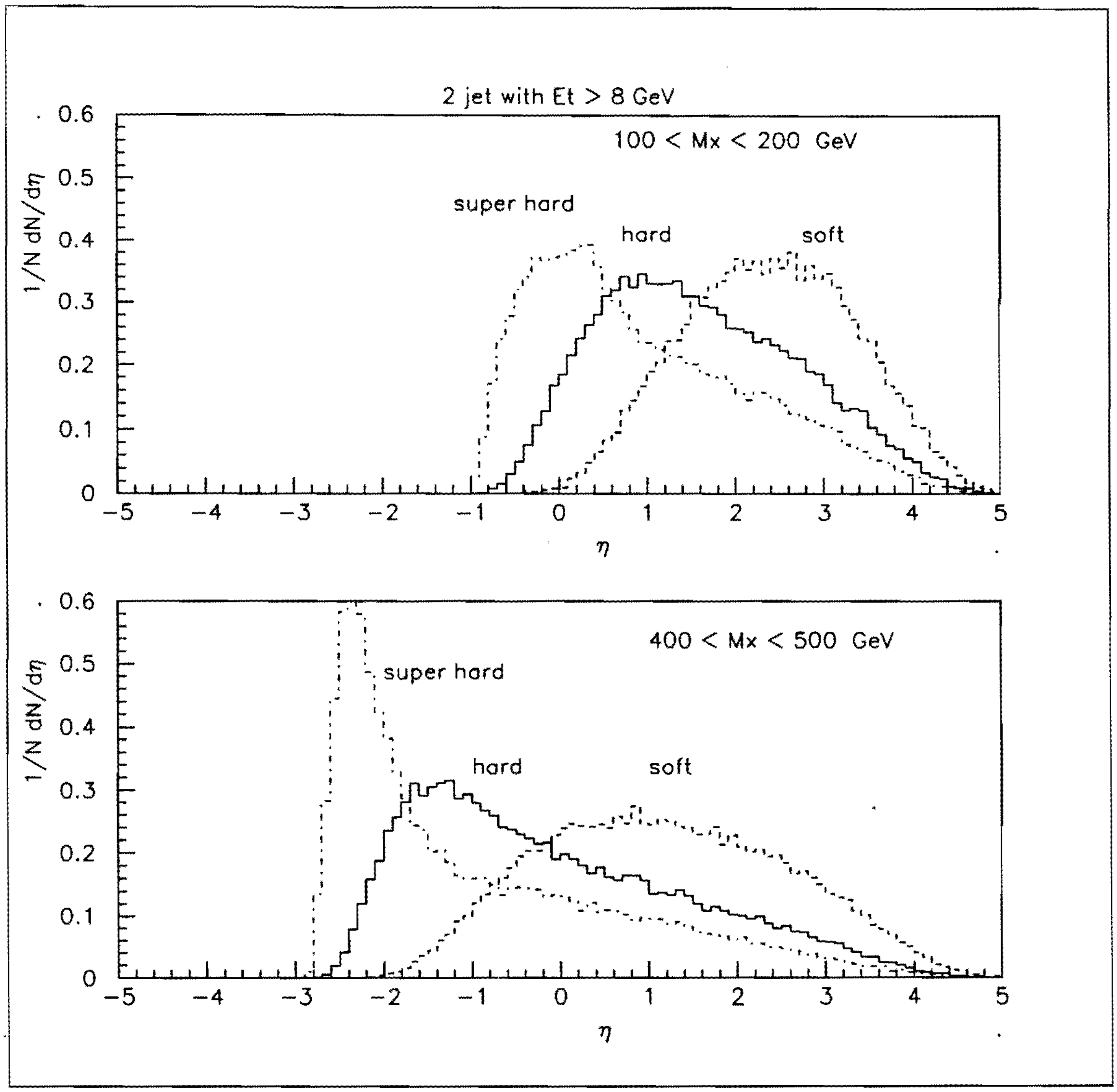

Figure 12: η_{jet} **distributions for two ranges of diffractive mass for superhard, hard and soft pomerons.**

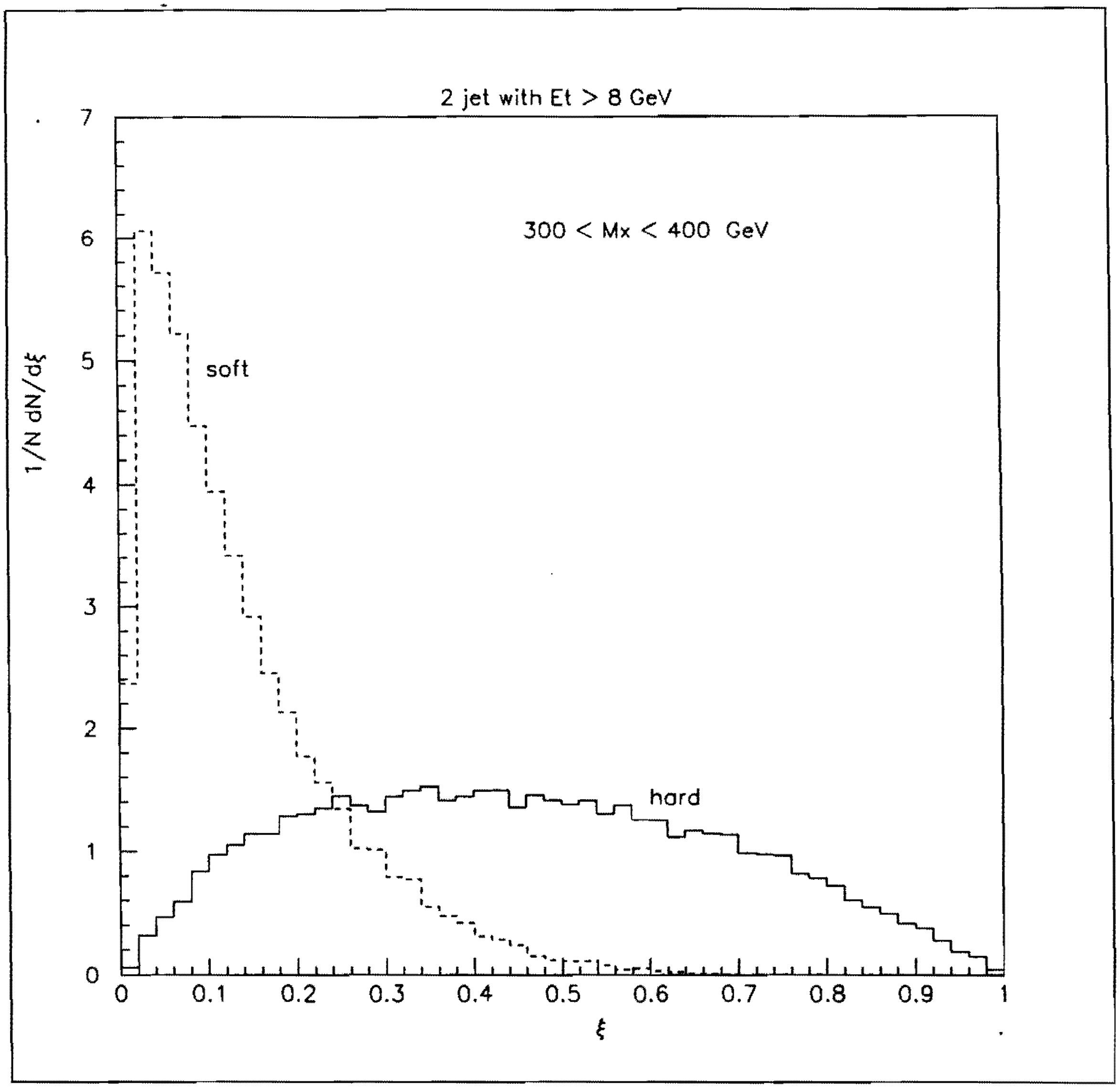

Figure 13: Distribution of the fractional momentum of the parton in the pomeron for soft and hard pomerons (the variable ξ is not to be confused with the momentum fraction of the pomeron in the proton).